Organic & Biomolecular Chemistry

ROYAL SOCIETY OF CHEMISTRY

PAPER

View Article Online
View Journal | View Issue

Check for updates

Cite this: *Org. Biomol. Chem.*, 2023, **21**, 7358

Evaluation of bioorthogonally applicable tetrazine–Cy3 probes for fluorogenic labeling schemes†

Evelin Albitz, [a,b] Krisztina Németh, [a] Gergely Knorr *[a] and Péter Kele *[a]

Received 31st July 2023,
Accepted 22nd August 2023

DOI: 10.1039/d3ob01204b

rsc.li/obc

The fluorogenic features of three sets of tetrazine–Cy3 probes were evaluated in bioorthogonal tetrazine–cyclooctyne ligation schemes. These studies revealed that the more efficient, internal conversion-based quenching of fluorescence by the tetrazine modul is translated to improved fluorogenicity compared to the more conventional, energy transfer-enabled design. Furthermore, a comparison of directly conjugated probes and vinylene-linked tetrazine–Cy3 probes revealed that more intimate conjugation of the tetrazine and the chromophore results in more efficient IC-based quenching even in spectral ranges where tetrazine exhibits diminished modulation efficiency. The applicability of these tetrazine-quenched fluorogenic Cy3 probes was demonstrated in the fluorogenic labeling schemes of the extra- and intracellular proteins of live cells.

Introduction

Recent advances in optical microscopy techniques have highlighted the profound implications of bioorthogonally applicable fluorogenic probes particularly in the context of live cell imaging schemes. The fluorescence of such probes is generally quenched by a rationally installed bioorthogonal motif (*e.g.*, azide[1] or tetrazine[2]), whose transformation in a highly specific ligation scheme results in a considerable increase in emission intensity at a given wavelength.[3] In combination with synthetic biology approaches, such as genetic code expansion for the installation of non-canonical amino acids (ncAAs[4]) bearing bioorthogonal functional groups or fusion protein technology to bind bioorthogonalized substrates of Halo-,[5] CLIP-[6] and SNAP-tags[7] covalently, bioorthogonal labeling schemes have become a powerful method for the site-specific and selective labeling of intra- and extracellular proteins of interest (POIs). From a super-resolution microscopy perspective, the minimal linkage error in the case of labeling schemes of ncAA-tagged POIs with a small-molecular probe is notable.[8,9] Amongst bioorthogonal reactions, inverse electron demand Diels–Alder (IEDDA) reactions of tetrazines and strained cycloalkynes/alkenes are extremely useful due to the fast kinetics of such transformations.[10,11] Furthermore, the tetrazine moiety is also capable of quenching the emission of fluorescent cores. Consequently, various tetrazine-quenched fluorogenic probes have been developed.[2,12–20] Tetrazines can exert their quenching effects through several mechanisms. These include photoinduced electron transfer (PET[12]) or energy transfer (FRET, TBET) processes.[14–20] These concepts have been successfully applied to various fluorophores (*e.g.* coumarin,[12] BODIPY,[13,16] phenoxazine,[18] xanthene,[14] and cyanine[21]). The quenching efficiency of the tetrazine, which is reflected in the increase in fluorescence intensity upon the IEDDA reaction, however, varies greatly. In general, tetrazines are more efficient in terms of quenching in the case of fluorophores emitting in the blue–green region of the spectrum, while fluorogenicity (*i.e.*, I/I_0) drops sharply upon entering the yellow regime.[22] Recently, several novel approaches have emerged to improve the fluorogenicity of probes emitting in the biologically more benign wavelength range. These approaches include multiple fluorogenicity[23] or energy transfer *via* Dexter mechanism.[24] Recently, our group reported on the development of fluorogenic dyads with improved yellow–red fluorogenicity due to an energy transfer-based relay mechanism.[25] At the same time, He and co-workers presented a set of red-emitting BODIPY–tetrazine probes with high turn-on values due to a twisted intramolecular charge transfer quenching mechanism,[26] while the Wu group showed examples of excellent fluorogenic probes by installing an amino-tetrazine at the *meso*-position of several

[a]*Chemical Biology Research Group, Institute of Organic Chemistry, Research Centre for Natural Sciences, Magyar tudósok krt. 2, H-1117 Budapest, Hungary. E-mail: kele.peter@ttk.hu*

[b]*Hevesy György PhD School of Chemistry, Eötvös Loránd University, Pázmány Péter sétány 1/a, H-1117 Budapest, Hungary*

†Electronic supplementary information (ESI) available: Experimental details, synthetic procedures, spectroscopic characterization, physical data determination, details of the imaging experiments, further images and viability assessment. See DOI: https://doi.org/10.1039/d3ob01204b

NIR-emitting cores.[27] These strategies indeed resulted in improved fluorogenic features, however, at the cost of synthetic ease.

Park and co-workers described monochromophoric systems, in which the tetrazine is an integral part of the π-system of a Seoul-Fluor chromophore. In this design, the excited chromophore relaxes to a lower-lying dark state corresponding to the n–π* transition of the tetrazine *via* internal conversion.[20] Later, a similar non-radiative, internal conversion-based relaxation pathway was proposed by us for vinyl-tetrazine-appended coumarin fluorophores and photocages.[15,28] While this robust quenching mechanism efficiently modulates UV or blue-excitable cores, it has limitations in red-absorbing chromophores due to the energy levels of the corresponding excited states.[27,29] Cyanines are very popular probes in the field of fluorescence imaging due to their high brightness and readily tuneable photophysical properties;[30] therefore cyanine probes with improved fluorogenic behavior are always welcomed by the scientific community, especially if an appended bioorthogonal moiety facilitates the specific ligation of such probes to target structures. Not long ago, we reported on two sets of tetrazine-functionalized cyanine probes.[21] We have found that in the case of probes that link the cyanine to the tetrazine through a phenylene motif (TBET design), the fluorogenic performance is lower (*i.e.*, 4× increase) compared to probes where a vinylene linkage was applied (*i.e.*, 14× increase). Since the vinylene linker allows direct conjugation of the tetrazine and the cyanine, the improved fluorogenic behaviour was attributed to a more efficient quenching mechanism that involves internal conversion to a dark, low-lying n–π* transition-derived excited state of the tetrazine. We wished to elaborate whether a more intimate connection between the tetrazine and the cyanine core allows improved fluorogenic behavior.

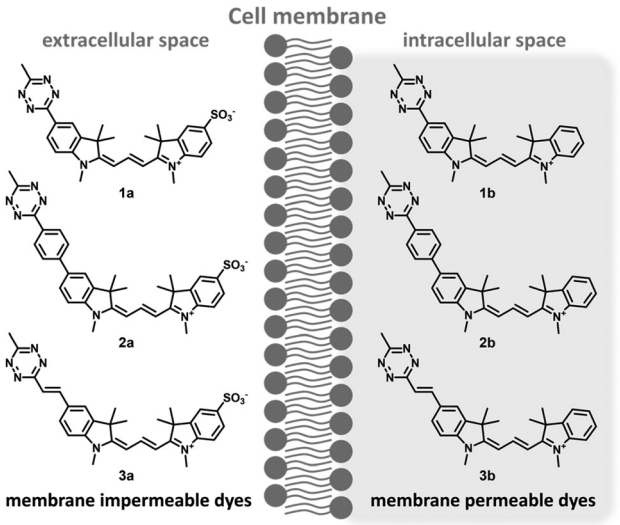

Fig. 1 Structures of bioorthogonally applicable fluorogenic cyanines **1–3**.

Results and discussion

Synthesis of fluorogenic probes

Along these considerations, we designed and synthesized three sets of Cy3 probes representing directly conjugated (**1**), phenylene-linked (**2**) and vinylene-linked (**3**) tetrazine–Cy3 scaffolds (Fig. 1). Each set included a presumably membrane permeable positively charged derivative and a non-membrane permeable congener with zero net charge. In order to access these probes, 4-aminobenzonitrile and 4-iodoaniline were first converted into 4-cyanophenylhydrazine (**S1**) and 4-iodophenylhydrazine (**S5**) in a diazotization-reduction sequence. Then, the indoles (**S2**, **S3** and **S6**) were prepared from the hydrazines in the presence of 3-methylbutan-2-one by a Fischer reaction. Intermediate **4** was obtained in moderate yields from indole **S2**. Treatment of the indoles (**4**, **S3**, **S6** or 2,3,3-trimethyl-3*H*-indole) with methyl iodide produced indolium precursors **5**, **S4**, **S7** and **S8**. Indolium salts **S4** and **S8** were converted into hemicyanines upon treatment with *N*,*N*′-diphenylformimidamide in a mixture of acetic acid and acetic anhydride. The subsequent reaction of the respective hemicyanine with indolium **5** or **S7** provided probes **1a–b** and cyanines **6a–b**. Intermediates **6a–b** were subjected to Suzuki- and Heck-type cross-coupling reactions to furnish probes **2a–b** and **3a–b**, respectively (Scheme 1).

Fluorescence and fluorogenicity studies

Next, we studied the main spectral features and fluorogenic behavior of our probes in an IEDDA reaction with (1*R*,8*S*,9*S*)-bicyclo[6.1.0]non-4-yn-9-ylmethanol, BCN (Table 1). As expected, the vinylene-linked derivatives (**3**) exhibited red-shifted absorption and emission spectra compared to **1** and **2**, due to the extension of the π system. In each case, the reaction with BCN resulted in a slight blue shift of the absorption and emission maxima with the exception of **3b**, where a small red shift was observed for λ_{em}. A small drop in the molar absorptivities was also detected upon reaction with BCN. The clicked products were found to be more fluorescent than their respective tetrazine congeners and the fluorescence quantum yields outweighed the decrease in the molar absorptivities, leading to brighter clicked products in each case. Very small effects on the spectral properties could be attributed to the presence of the sulfonate substituent. A comparison of the fluorescence enhancement values of the different designs revealed considerable differences of the turn-on performances. In line with our hypothesis, the highest fluorogenicity (~20×) was observed for intimately conjugated tetrazine–cyanines, while vinylene conjugation or phenylene linkage gave lower enhancement values.

To gain further insight into the quenching mechanism, we conducted TD-DFT calculations at the B3LYP/6-31+G(d) level for molecules **1a**, **1b**, **3a**, and **3b**. In all cases, we found that the main excitation pathway is an $S_0 \rightarrow S_2$ transition (see the ESI; Fig. S10–S13†). The S_1 (LUMO) orbital was found to be localized mostly on the tetrazine and to a lesser extent on the cyanine scaffold. At the same time, the S_2 (LUMO+1) molecular

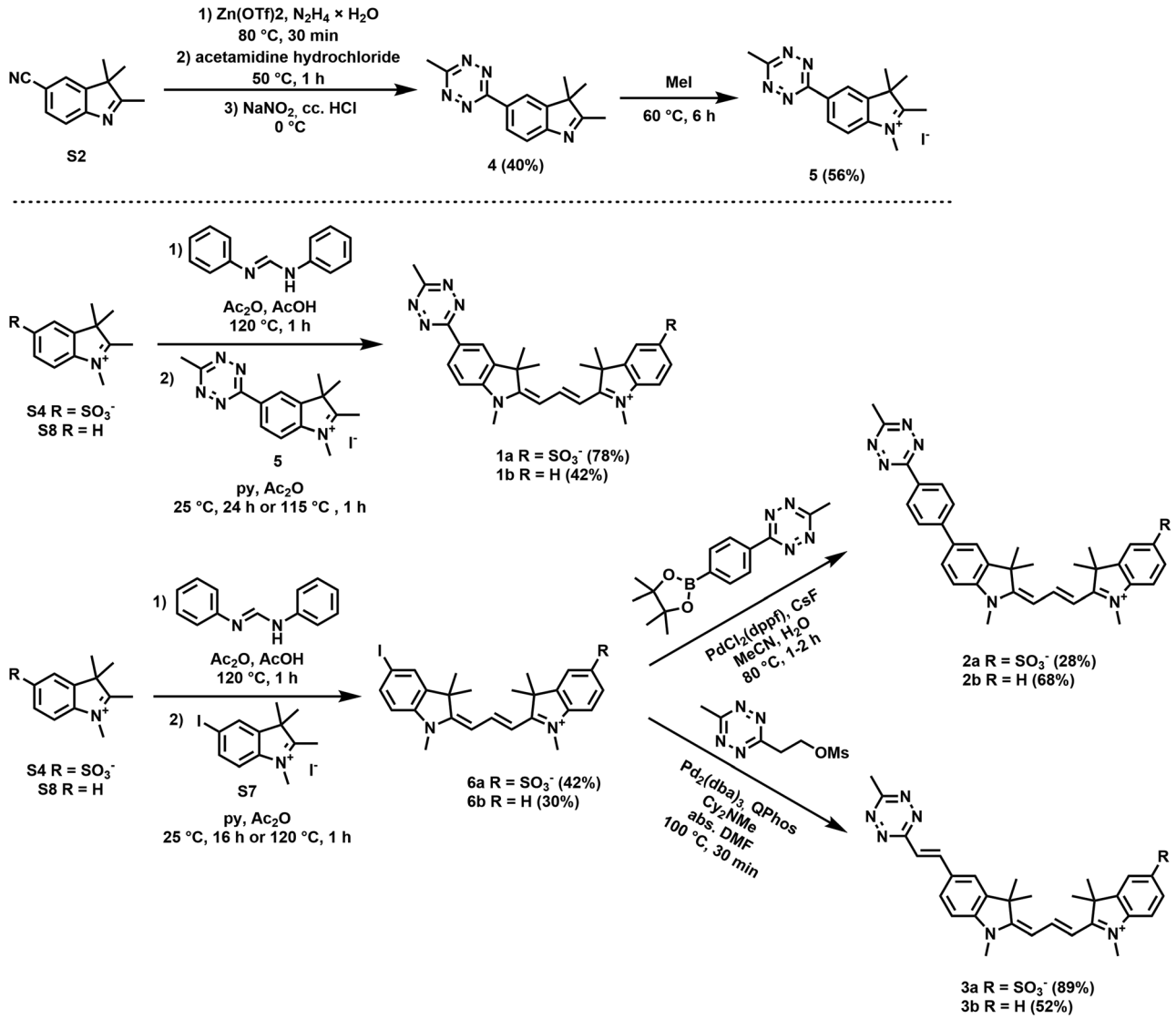

Scheme 1 Synthesis of fluorogenic cyanines **1–3**.

orbital was delocalized all over the molecule. These two excited state orbitals, however, were very close to each other; in fact, they were separated only by 0.05–0.16 eV, which is within the error limit of the calculation method.[31] This implies that although the S_2 state is formed predominantly corresponding to a π–π* transition of the cyanine unit as suggested by the oscillator strengths, the transition between the S_1 and S_2 excited states is reversible. These findings not only explain why conjugated Cy3–tetrazines are more fluorogenic than TBET-governed probes (*e.g.*, **2a** and **2b**) but also justify the lower fluorogenicity of **1** and **3** compared to, *e.g.*, related coumarin or Seoul-Fluor probes.

Confocal and STED microscopy

The notable increase in brightness in the case of directly conjugated tetrazine–Cy3 probes **1a–b** upon IEDDA reactions suggests that these are promising candidates for *in vivo* labeling schemes. For comparison, probes **3a–b** were also included in these studies. Before applying the probes to live cells, we evaluated the effects of the probes on cellular viability. Treatment of HEK293T cells with probes **1a–b** or **3a–b** even for prolonged incubation times (*i.e.*, 90 minutes) either did not have any noticeable effects on viability or affected the cells only negligibly (*e.g.*, the changes in viabilities remained within the error range) in the applied 0.3–3 μM concentration range (see the ESI; Fig. S9† for more details).

For extracellular protein labeling schemes, we modified the GFP-fused insulin receptor (IR) protein site specifically with a bioorthogonalized lysine (ε-amino(BCN)-Lys) at the extracellular domain using genetic code expansion. We then treated $IR^{K676BCN\text{-}Lys}$–GFP-expressing live HEK293T cells with probes **1a** and **3a**. After a 90-minute incubation time, the cells were washed, fixed, and subjected to confocal microscopy (Fig. 2). To our delight, fluorogenic cyanines **1a** and **3a** were indeed

Table 1 Main photophysical data of cyanine dyes and their BCN conjugates[a]

	λ_{abs} (nm)	λ_{em} (nm)	$\varepsilon^b \times 10^4$ (M^{-1} cm^{-1})	Φ^c (%)	$B \times 10^4$ ($\varepsilon \times \phi$)	I_{BCN}/I_{Tet}[d]	B_{BCN}/B_{Tet}
1a	565	578	11.5	1.63	18.8	21.0	12.4
1a·BCN	558	571	10.6	21.92	232.3		
1b	561	575	8.2	1.13	9.2	19.3	12.8
1b·BCN	555	570	7.8	15.18	118.2		
2a	568	586	14.0	3.19	44.8	4.3	4.0
2a·BCN	567	586	13.2	13.56	179.3		
2b	567	587	13.2	2.94	38.9	5.8	5.3
2b·BCN	565	585	12.8	16.22	207.7		
3a	578	593	16.3	0.97	15.8	11.9	9.0
3a·BCN	575	596	14.0	10.19	142.6		
3b	577	584	11.5	2.91	33.5	6.1	4.4
3b·BCN	572	592	10.7	13.80	148.0		

[a] In sodium PBS (pH = 7.4, containing 0.1% SDS). [b] Determined at $\lambda_{abs,max}$. [c] Relative to rhodamine B (ϕ = 0.65). [d] Determined at $\lambda_{em,max}$ of the BCN conjugate.

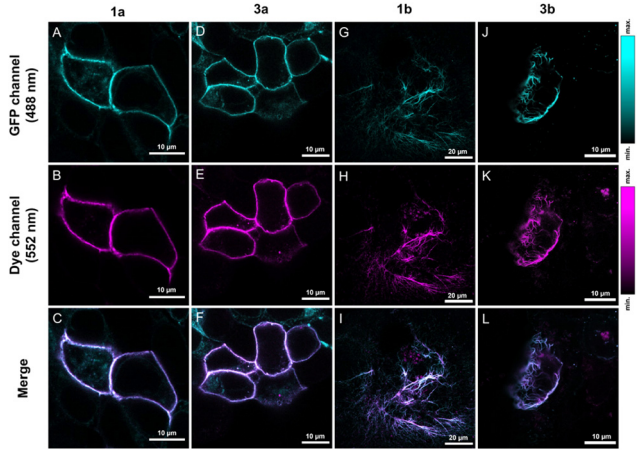

Fig. 2 Confocal microscopy images of $IR^{K676BCN\text{-}Lys}$–GFP expressing HEK293T cells (A–F) and $Vim^{N116BCN\text{-}Lys}$–GFP expressing COS-7 cells (G–L) treated with BCN–Lys and probes **1a** (A–C), **1b** (G–I), **3a** (D–F) and **3b** (J–L). Spectral detection: GFP: λ_{exc}: 488/λ_{em}: 500–540 nm; dye: λ_{exc}: 552/λ_{em}: 565–800 nm. Overlay pictures demonstrate the merged fluorescent signals of the reporter and dye.

membrane impermeable and suitable for selective extracellular labeling and showed excellent co-localization with the reporter protein. We also tested the applicability of the non-sulfonated cyanines (**1b** and **3b**) in the labeling schemes of intracellular proteins. To this end, we labeled a similarly tailored, genetically bioorthogonalized cytoskeletal protein, vimentin–GFP, modified with BCN-Lys. Live COS-7 cells expressing a $Vim^{N116BCN\text{-}Lys}$–GFP protein construct were treated with **1b** and **3b** for 90 minutes, washed, fixed and then imaged (Fig. 2). The low background and the excellent co-localization of the fluorescent signals with that of the reporter protein confirmed the membrane permeability of the probes and their suitability for specific fluorogenic labeling schemes.

We also wished to demonstrate the applicability of the dyes in super-resolution (STED) microscopy. The well-known spectral properties of the Cy3 dyes[25] suggest that these probes are suitable for STED microscopy equipped with a 660 nm depletion laser. We first assessed the photostability of probes **1** and **3** by multiple frame acquisition. Neither **1b** nor **3b** showed significant decrease in intensity over the 160-cycle period, while a slight decrease was observed for probes **1a** and **3a** compared to their initial values (see the ESI; Fig. S7†) suggesting the suitability of probes **1a–b** and **3a–b** in STED

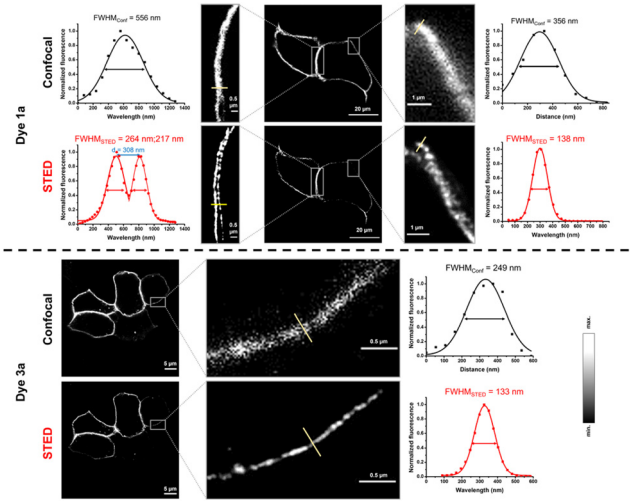

Fig. 3 Confocal and STED images of $IR^{K676BCN\text{-}Lys}$–GFP expressing HEK293T cells treated with BCN–Lys and dye **1a** and **3a**. λ_{exc}: 552/λ_{em}: 565–800 nm; λ_{STED}: 660 nm (CW). FWHM: full width at half maxima.

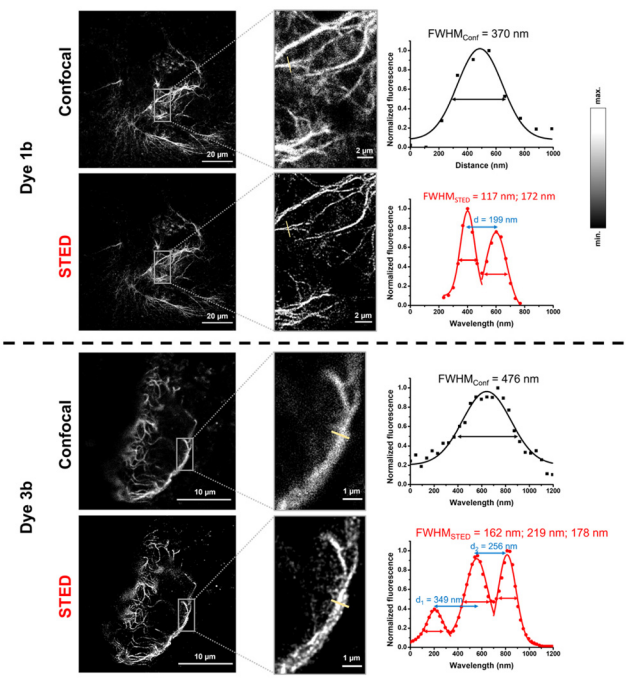

Fig. 4 Confocal and STED images of $Vim^{N116BCN\text{-}Lys}$–GFP expressing COS7 cells treated with BCN-Lys and dye **1b** and **3b**. λ_{exc}: 552/λ_{em}: 565–800 nm; λ_{STED}: 660 nm (CW). FWHM: full width at half maxima.

imaging. Indeed, a more detailed structure of the vimentin network was revealed by applying membrane-permeable **1b** and **3b**, and a more detailed image of the membrane lineage between two neighboring cells was acquired when using non-permeable **1a** and **3a**. Overall, the resolution characterised by the full width at half maximum (FWHM) values increased by a factor of 2–3 upon STED imaging with probes **1a–b** and **3a–b** (Fig. 3 and 4).

Conclusions

In conclusion, we synthesized three sets of tetrazine-functionalized Cy3 derivatives following different design strategies in order to gain experimental insights into the modulation effects of the bioorthogonal unit on the fluorescence of yellow-emitting indocyanines. Our study involved directly conjugated tetrazine–cyanines (direct conjugation, **1a–b**), phenylene-linked units (TBET design, **2a–b**) or vinylene-conjugated systems (π-extended direct conjugation, **3a–b**). Each of these sets included a membrane-permeable derivative and a non-permeable derivative. We assessed the fluorogenic characteristics of **1–3** upon reacting these probes with a strained cyclooctyne, BCN, in an IEDDA reaction. A comparison of the fluorogenicities revealed that probes **1a–b** outperformed probes **2a–b** and **3a–b**, indicating that the more intimate conjugation of the tetrazine results in more efficient quenching of fluorescence and further confirming that internal conversion-based modulation of fluorescence is more efficient than the through-bond energy transfer-based modulation mechanism. The directly conjugated probes **1** and **3** were further evaluated in the labeling schemes of genetically bioorthogonalized extra- and intracellular proteins of live cells. To our delight, all these probes were found to be suitable for the specific labeling of target structures. Furthermore, all four probes tested were found to be applicable for STED imaging, resulting in subdiffraction imaging of extracellular insulin receptors or the intracellular vimentin network. These results indicate that fluorogenic probes quenched *via* internal conversion can even be effective in spectral ranges where the tetrazine exhibits diminished modulation efficiency.

Experimental

Organic synthesis

General methods. All starting materials were obtained from commercial suppliers (Sigma-Aldrich, Fluka, Merck, Alfa Aesar, Reanal, Molar Chemicals, and Fluorochem) and used without further purification. Analytical thin-layer chromatography (TLC) was performed on silica gel 60 F_{254}-precoated aluminum TLC plates from Merck. Flash column chromatography was performed on a Teledyne ISCO COMBI Flash Nextgen 300+ automated flash chromatographer with silica gel (25–40 μm) from Zeochem or a RediSep® Rf C18 High Performance GOLD column. Microwave experiments were performed on an AntonPaar Monowave 400 microwave reactor using sealed tubes and for each experiment, fast heating to 100 °C was performed and the temperature was maintained constant for one hour. NMR spectra were recorded on a Varian Inova 500 MHz and Varian Inova 300 MHz spectrometer. Chemical shifts (δ) are given in parts per million (ppm) using solvent signals as the reference. Coupling constants (J) are reported in hertz (Hz). Analytical RP-HPLC-UV/Vis-MS experiments were performed on a SHIMADZU LCMS-2020 system by using a Phenomenex Kinetex EVO C18 column (50 × 2.10 mm I.D.) with 2.6 μm silica (100 Å pore size) as the stationary phase with a photodiode array UV/Vis detector (λ = 190–800 min 0% B) with eluents A (95% H_2O, 5% MeCN, and 0.1% HCOOH) and B (95% MeCN, 5% H_2O, and 0.1% HCOOH) and an ESI-MS detector. The linear gradient elution method was employed at a flow rate of 1.0 mL min^{-1} at 40 °C. The samples were dissolved in a MeCN–H_2O mixture. Semipreparative HPLC was performed on a Wufeng Chrom LC100 HPLC system using a Gemini C18 column (150 × 21 mm I.D.) with 5 μm silica (110 pore size) as the stationary phase. Spectroscopic measurements were performed on a Jasco FP 8300 spectrofluorometer and a JASCO v750 spectrophotometer in all-sodium PBS (pH = 7.4, containing 0.1% SDS) at r.t. Quartz cuvettes with a path length of 1 cm were used.

The exact masses were determined with an Agilent 6230 time-of-flight mass spectrometer.

Synthesis of 2,3,3-trimethyl-5-(6-methyl-1,2,4,5-tetrazin-3-yl)-3*H*-indole (4). Indole **S2** (1.00 g, 5.4 mmol, 1.0 equiv.) and Zn $(OTf)_2$ (0.986 g, 2.72 mmol, 0.5 equiv.) were dissolved in hydrazine monohydrate (13.5 mL, 271.5 mmol, 50 equiv.) and stirred at 80 °C for 30 minutes. Then, the reaction mixture was cooled to 50 °C and acetamidine hydrochloride (5.13 g, 54.30 mmol, 10.0 equiv.) was added portionwise for 1 hour. After cooling to 0 °C, the mixture was diluted with 50 mL of ethyl acetate and 50 mL of water, and then $NaNO_2$ (3.70 g, 54.3 mmol, 10.0 equiv.) was added. With vigorous stirring, AcOH was added dropwise to set pH = 3. The two phases were separated, and the aqueous layer was extracted with ethyl acetate three times. The combined organic layers were extracted with cc. $NaHCO_3$ solution three times, dried over $MgSO_4$, and evaporated under vacuum. The crude product was purified by flash chromatography on silica gel (dichloromethane–methanol 0 to 10%) to yield 550 mg (40%) of the pink solid compound. ^{1}H NMR (500 MHz, $CDCl_3$) δ 8.60 (dd, J = 8.1, 1.7 Hz, 1H), 8.52 (d, J = 1.3 Hz, 1H), 7.71 (d, J = 8.1 Hz, 1H), 3.08 (s, 3H), 2.35 (s, 3H), 1.40 (s, 6H). ^{13}C NMR (126 MHz, $CDCl_3$) δ 191.6, 167.0, 164.4, 157.8, 146.9, 128.8, 128.5, 121.1, 120.8, 54.3, 23.1, 21.2, 15.9. HRMS: m/z calcd for $[C_{14}H_{16}N_5]^+$: 254.1400; found: 254.1402 $[M + H]^+$.

Synthesis of 1,2,3,3-tetramethyl-5-(6-methyl-1,2,4,5-tetrazin-3-yl)-3*H*-indol-1-ium iodide (5). In a pressure tube, indole **4** (200 mg, 0.790 mmol, 1 equiv.) was dissolved in methyl iodide (1475 μL, 23.690 mmol, 30 equiv.) and reacted at 60 °C for 6 hours. After cooling to room temperature, ethyl acetate was added and the resulting precipitate was filtered, washed with

cold ethyl acetate and dried to yield 223 mg (71%) of the dark red solid compound. The product was used without further purification. ^{1}H NMR (500 MHz, DMSO-d_6) δ 8.91 (s, 1H), 8.72 (d, J = 8.2 Hz, 1H), 8.20 (d, J = 8.3 Hz, 1H), 4.06 (s, 3H), 3.04 (s, 3H), 2.86 (s, 3H), 1.65 (s, 6H). ^{13}C NMR (126 MHz, DMSO-d_6) δ 199.0, 167.8, 163.3, 145.5, 143.2, 133.4, 128.9, 122.8, 116.7, 55.0, 35.6, 22.1, 21.4, 15.1. HRMS: m/z calcd for $[C_{15}H_{18}N_5]^+$: 268.1556; found: 268.1560 $[M]^+$.

Synthesis of 1,3,3-trimethyl-2-(3-(1,3,3-trimethyl-5-(6-methyl-1,2,4,5-tetrazin-3-yl)indolin-2-ylidene)prop-1-en-1-yl)-3*H*-indol-1-ium-5-sulfonate (1a). Compound **S4** (48 mg, 0.190 mmol, 2.5 equiv.) and *N*,*N*′-diphenylformamidine (60 mg, 0.304 mmol, 4.0 equiv.) were reacted in a mixture of 500 μL of acetic acid and 500 μL of acetic anhydride at 120 °C for 1 hour. The reaction mixture was cooled to room temperature, 10 mL of ethyl acetate was added, and the precipitate was filtered, washed with ethyl acetate and dried. This intermediate hemi-cyanine was dissolved in 3 mL of pyridine; compound **5** (30 mg, 0.076 mmol, 1.0 equiv.) and 500 μL of acetic anhydride were added and stirred at 25 °C for 24 hours. Then 10 mL of ethyl acetate was added; the precipitate was filtered and washed with ethyl acetate. The crude product was purified by flash chromatography on silica gel (dichloromethane–methanol 0 to 20%) to yield 31 mg (78%) of purple crystals. Before spectroscopic measurements, the product was further purified by preparative HPLC (water–acetonitrile starting from 95 : 5 to 0 : 100). ^{1}H NMR (500 MHz, CD_3OD) δ 8.77 (d, J = 1.2 Hz, 1H), 8.75 (dd, J = 8.4, 1.6 Hz, 1H), 8.70 (t, J = 13.5 Hz, 1H), 8.05 (d, J = 1.4 Hz, 1H), 8.01 (dd, J = 8.3, 1.6 Hz, 2H), 7.65 (d, J = 8.4 Hz, 1H), 7.51 (d, J = 8.3 Hz, 1H), 6.62 (d, J = 13.6 Hz, 1H), 6.58 (d, J = 13.3 Hz, 1H), 3.82 (s, 3H), 3.82 (s, 3H), 3.13 (s, 3H), 1.94 (s, 6H), 1.89 (s, 6H). ^{13}C NMR (126 MHz, CD_3OD) δ 178.3, 176.9, 168.6, 165.0, 153.0, 145.2, 144.6, 143.1, 142.3, 130.6, 130.2, 130.2, 128.3, 122.6, 121.4, 112.8, 112.3, 105.5, 104.6, 51.0, 50.5, 32.2, 31.9, 28.3, 28.0, 21.1. HRMS: m/z calcd for $[C_{28}H_{31}N_6O_3S]^+$: 531.2172; found: 531.2177 $[M + H]^+$.

Synthesis of 1,3,3-trimethyl-2-(3-(1,3,3-trimethyl-5-(6-methyl-1,2,4,5-tetrazin-3-yl)indolin-2-ylidene)prop-1-en-1-yl)-3*H*-indol-1-ium formate (1b). Compound **S8** (48 mg, 0.158 mmol, 2.5 equiv.) and *N*,*N*′-diphenylformamidine (50 mg, 0.253 mmol, 4.0 equiv.) were reacted in a mixture of 500 μL of acetic acid and 500 μL of acetic anhydride at 120 °C for 1 hour. The reaction mixture was cooled to room temperature, 10 mL of ethyl acetate was added, and the precipitate was filtered, washed with ethyl acetate and dried. This intermediate hemi-cyanine was dissolved in 1 mL of pyridine; compound **5** (25 mg, 0.0633 mmol, 1.0 equiv.) and 100 μL of acetic anhydride were added and stirred at 115 °C for 1 hour. After cooling to room temperature, the solvents were evaporated under vacuum. The residue was purified by flash chromatography on silica gel (dichloromethane–methanol 0 to 20%). Before spectroscopic measurements the product was further purified by preparative HPLC (water–acetonitrile containing 0.1% HCOOH starting from 95 : 5 to 0 : 100) to yield 13.2 mg (42%) of purple crystals. ^{1}H NMR (500 MHz, CD_3OD) δ 8.76–8.73 (m, 2H), 8.68 (t, J = 13.5 Hz, 1H), 7.66 (d, J = 7.4 Hz, 1H), 7.61 (d, J = 8.9 Hz, 1H), 7.56 (d, J = 7.9 Hz, 1H), 7.51 (d, J = 7.8 Hz, 1H), 7.45 (t, J = 7.4 Hz, 1H), 6.63 (d, J = 13.7 Hz, 1H), 6.52 (d, J = 13.2 Hz, 1H), 3.83 (s, 3H), 3.72 (s, 3H), 3.12 (s, 3H), 1.94 (s, 6H), 1.87 (s, 6H). ^{13}C NMR (126 MHz, CD_3OD) δ 178.2, 175.9, 168.6, 165.0, 152.5, 143.9, 142.9, 142.5, 130.2, 130.2, 130.1, 127.6, 123.5, 122.6, 112.9, 112.5, 105.5, 103.8, 73.7, 71.5, 62.2, 51.2, 32.2, 28.4, 28.0, 21.0. HRMS: m/z calcd for $[C_{28}H_{31}N_6]^+$: 451.2610; found: 451.2612 $[M + H]^+$.

Synthesis of 2-(3-(5-iodo-1,3,3-trimethylindolin-2-ylidene)prop-1-en-1-yl)-1,3,3-trimethyl-3*H*-indol-1-ium-5-sulfonate (6a). Compound **S4** (400 mg, 1.58 mmol, 2.0 equiv.) and *N*,*N*′-diphenylformamidine (620 mg, 3.16 mmol, 4.0 equiv.) were reacted in a mixture of 2.5 mL of acetic acid and 2.5 mL of acetic anhydride at 120 °C for 1 hour. The reaction mixture was cooled to room temperature, 50 mL of ethyl acetate was added, and the precipitate was filtered, washed with ethyl acetate and dried. This intermediate hemi-cyanine was dissolved in 10 mL of pyridine; compound **S7** (258 mg, 0.79 mmol, 1.0 equiv.) and 1 mL of acetic anhydride were added and stirred at 25 °C for 16 hours. Then, 50 mL of ethyl acetate was added, and the precipitate was filtered and washed with ethyl acetate. The crude product was purified by flash chromatography on silica gel (dichloromethane–methanol 0 to 20%) to yield 187 mg (42%) of purple crystals. ^{1}H NMR (500 MHz, DMSO-d_6) δ 8.32 (t, J = 13.5 Hz, 1H), 8.01 (d, J = 1.6 Hz, 1H), 7.81 (d, J = 1.4 Hz, 1H), 7.77 (dd, J = 8.3, 1.6 Hz, 1H), 7.69 (dd, J = 8.2, 1.5 Hz, 1H), 7.41 (d, J = 8.3 Hz, 1H), 7.27 (d, J = 8.4 Hz, 1H), 3.66 (s, 3H), 3.60 (s, 3H), 1.69 (s, 6H), 1.68 (s, 6H). ^{13}C NMR (126 MHz, DMSO-d_6) δ 175.1, 173.4, 149.5, 146.0, 142.8, 142.6, 142.5, 140.0, 137.0, 131.0, 126.1, 119.7, 113.5, 110.7, 103.5, 102.6, 89.2, 49.0, 48.7, 31.6, 31.3, 27.1. HRMS: m/z calcd for $[C_{25}H_{28}IN_2O_3S]^+$: 563.0859; found: 563.0845 $[M + H]^+$.

Synthesis of 2-(3-(5-iodo-1,3,3-trimethylindolin-2-ylidene)prop-1-en-1-yl)-1,3,3-trimethyl-3*H*-indol-1-ium formate (6b). Compound **S8** (700 mg, 2.33 mmol, 1.55 equiv.) and *N*,*N*′-diphenylformamidine (913 mg, 4.65 mmol, 3.1 equiv.) were reacted in a mixture of 3 mL of acetic acid and 3 mL of acetic anhydride at 120 °C for 1 hour. The reaction mixture was cooled to room temperature, 50 mL of ethyl acetate was added, and the precipitate was filtered, washed with ethyl acetate and dried. This intermediate hemi-cyanine was dissolved in 10 mL of pyridine; compound **S7** (640 mg, 1.50 mmol, 1.0 equiv.) and 1.5 mL of acetic anhydride were added and stirred at 120 °C for 1 hour. Then the solvents were evaporated under vacuum. The residue was purified by flash chromatography on silica gel (dichloromethane–methanol 0 to 2%) to yield 279 mg (30%) of purple crystals. Before NMR measurements, the product was further purified by preparative HPLC (water–acetonitrile containing 0.1% HCOOH starting from 95 : 5 to 0 : 100). ^{1}H NMR (500 MHz, DMSO-d_6) δ 8.31 (t, J = 13.5 Hz, 1H), 8.15 (s, 1H), 8.03 (d, J = 1.4 Hz, 1H), 7.78 (dd, J = 8.3, 1.5 Hz, 1H), 7.65 (d, J = 7.4 Hz, 1H), 7.50 (d, J = 7.8 Hz, 1H), 7.46 (t, J = 7.6 Hz, 1H), 7.32 (t, J = 7.3 Hz, 1H), 7.27 (d, J = 8.4 Hz, 1H), 6.49 (d, J = 13.6 Hz, 1H), 6.40 (d, J = 13.4 Hz, 1H), 3.67 (s, 3H), 3.59 (s, 3H), 1.68 (s, 6H), 1.67 (s, 6H). ^{13}C NMR (126 MHz, DMSO-d_6) δ 174.9, 173.2, 163.0, 149.5, 142.8, 142.6, 142.6, 140.7, 137.0,

131.0, 128.6, 125.5, 122.4, 113.4, 111.7, 103.4, 102.4, 89.1, 49.0, 48.7, 31.5, 31.3, 27.2, 27.1. HRMS: *m*/*z* calcd for $[C_{25}H_{28}IN_2]^+$: 483.1297; found: 483.1288 $[M]^+$.

Synthesis of 1,3,3-trimethyl-2-(3-(1,3,3-trimethyl-5-(4-(6-methyl-1,2,4,5-tetrazin-3-yl)phenyl)indolin-2-ylidene)prop-1-en-1-yl)-3*H*-indol-1-ium-5-sulfonate (2a). A mixture of cyanine **6a** (30 mg, 0.053 mmol, 1.0 equiv.), 3-methyl-6-(4-(4,4,5,5-tetramethyl-1,3,2-dioxaborolan-2-yl)phenyl)-1,2,4,5-tetrazine[18] (32 mg, 0.107 mmol, 2.0 equiv.), Pd(dppf)Cl_2 (4 mg, 0.0055 mmol, 0.1 equiv.) and CsF (80 mg, 0.5267 mmol, 10.0 equiv.) was suspended in 1000 μL of acetonitrile and 100 μL of H_2O. The reaction mixture was stirred at 80 °C for 2 hours. The solvent was evaporated, and the crude product was purified by flash chromatography on silica gel (dichloromethane–methanol 0 to 20%) to yield 9 mg (28%) of purple crystals. Before spectroscopic measurements, the product was further purified by preparative HPLC (water–acetonitrile starting from 95 : 5 to 0 : 100). ^{1}H NMR (500 MHz, DMSO-d_6) δ 8.58 (d, J = 8.4 Hz, 2H), 8.38 (t, J = 13.5 Hz, 1H), 8.14 (s, 1H), 8.08 (d, J = 8.4 Hz, 2H), 7.92 (d, J = 8.2 Hz, 1H), 7.82 (s, 1H), 7.70 (d, J = 8.2 Hz, 1H), 7.59 (d, J = 8.4 Hz, 1H), 7.41 (d, J = 8.2 Hz, 1H), 6.48 (d, J = 13.5 Hz, 1H), 3.70 (s, J = 14.8 Hz, 3H), 3.67 (s, 3H), 3.02 (s, 3H), 1.78 (s, 6H), 1.72 (s, 6H). ^{13}C NMR (126 MHz, DMSO-d_6) δ 174.9, 174.2, 171.1, 167.0, 163.1, 149.4, 146.0, 144.8, 143.2, 142.9, 142.5, 141.5, 139.9, 135.8, 130.7, 127.9, 127.5, 127.3, 126.1, 121.0, 119.8, 111.9, 110.6, 103.3, 103.1, 48.9, 31.6, 27.3, 27.2, 20.8. HRMS: *m*/*z* calcd for $[C_{34}H_{35}N_6O_3S]^+$: 607.2485; found: 607.2498 $[M + H]^+$.

Synthesis of 1,3,3-trimethyl-2-(3-(1,3,3-trimethyl-5-(4-(6-methyl-1,2,4,5-tetrazin-3-yl)phenyl)indolin-2-ylidene)prop-1-en-1-yl)-3*H*-indol-1-ium formate (2b). A mixture of cyanine **6b** (50 mg, 0.0819 mmol, 1.0 equiv.), 3-methyl-6-(4-(4,4,5,5-tetramethyl-1,3,2-dioxaborolan-2-yl)phenyl)-1,2,4,5-tetrazine[18] (49 mg, 0.1638 mmol, 2.0 equiv.), Pd(dppf)Cl_2 (6 mg, 0.0082 mmol, 0.1 equiv.) and CsF (62 mg, 0.4095 mmol, 5.0 equiv.) was suspended in 2000 μL of acetonitrile and 200 μL of H_2O. The reaction mixture was stirred at 80 °C for 1 hour. The solvent was evaporated, and the crude product was purified by flash chromatography on silica gel (dichloromethane–methanol 0 to 20%). Before spectroscopic measurements, the product was further purified by preparative HPLC (water–acetonitrile containing 0.1% HCOOH starting from 95 : 5 to 0 : 100) to yield 32 mg (68%) of purple crystals. ^{1}H NMR (500 MHz, DMSO-d_6) δ 8.58 (d, J = 8.5 Hz, 2H), 8.37 (t, J = 13.5 Hz, 1H), 8.14 (d, J = 1.6 Hz, 1H), 8.08 (d, J = 8.5 Hz, 2H), 7.92 (dd, J = 8.4, 1.7 Hz, 1H), 7.65 (d, J = 7.3 Hz, 1H), 7.59 (d, J = 8.4 Hz, 1H), 7.52–7.43 (m, J = 8.1 Hz, 2H), 7.32 (td, J = 7.4, 1.5 Hz, 1H), 6.48 (apparent t containing: 6.50 (d, J = 13.7 Hz, 1H), 6.47 (d, J = 13.6 Hz, 1H)), 3.69 (s, 3H), 3.68 (s, 3H), 3.02 (s, 3H), 1.78 (s, 6H), 1.71 (s, 6H). ^{13}C NMR (126 MHz, DMSO-d_6) δ 174.7, 174.1, 167.0, 163.0, 149.4, 143.2, 143.0, 142.6, 141.4, 140.6, 135.7, 130.7, 128.5, 127.9, 127.5, 127.3, 125.3, 122.4, 121.0, 111.8, 111.6, 103.2, 102.9, 49.0, 48.8, 31.5, 27.3, 27.2, 20.8. HRMS: *m*/*z* calcd for $[C_{34}H_{35}N_6]^+$: 527.2923; found: 527.2922 $[M + H]^+$.

Synthesis of 1,3,3-trimethyl-2-(3-(1,3,3-trimethyl-5-((*E*)-2-(6-methyl-1,2,4,5-tetrazin-3-yl)vinyl)indolin-2-ylidene)prop-1-en-1-yl)-3*H*-indol-1-ium-5-sulfonate (3a). A mixture of cyanine **6a** (30 mg, 0.053 mmol, 1.0 equiv.), 2-(6-methyl-1,2,4,5-tetrazin-3-yl)ethyl methanesulfonate[19] (35 mg, 0.162 mmol, 3.0 equiv.), $Pd_2(dba)_3$ (2.4 mg, 0.0026 mmol, 0.05 equiv.), QPhos (1.9 mg, 0.0026 mmol, 0.05 equiv.), *N*,*N*-dicyclohexylmethylamine (35 μL, 0.162 mmol, 3.0 equiv.) and 2 mL of anhydrous dimethylformamide was purged with N_2 for 15 minutes. The reaction mixture was stirred at 100 °C for 30 minutes. The solvent was evaporated *in vacuo* and the crude product was purified by flash chromatography on silica gel (dichloromethane–methanol 0 to 20%) to yield 26 mg (89%) of purple crystals. Before spectroscopic measurements, the product was further purified by preparative HPLC (water–acetonitrile starting from 95 : 5 to 0 : 100). ^{1}H NMR (500 MHz, DMSO-d_6) δ 8.37 (t, J = 13.5 Hz, 1H), 8.31–8.27 (m, 2H), 7.91 (dd, J = 8.2, 0.8 Hz, 1H), 7.83 (d, J = 1.0 Hz, 1H), 7.72 (d, J = 16.2 Hz, 1H), 7.70 (dd, J = 8.1, 1.3 Hz, 1H), 7.51 (d, J = 8.3 Hz, 1H), 7.43 (d, J = 8.3 Hz, 1H), 6.51 (d, J = 13.6 Hz, 1H), 6.46 (d, J = 13.3 Hz, 1H), 3.69 (s, 3H), 3.66 (s, 3H), 2.96 (s, 3H), 1.76 (s, 6H), 1.72 (s, 6H). ^{13}C NMR (126 MHz, DMSO-d_6) δ 175.4, 173.8, 170.8, 165.9, 164.3, 149.5, 146.2, 144.2, 142.4, 141.3, 140.1, 139.2, 132.0, 130.2, 126.1, 121.4, 120.1, 119.8, 111.5, 110.8, 103.9, 103.2, 49.1, 48.5, 31.7, 27.3, 27.1, 20.8. HRMS: *m*/*z* calcd for $[C_{30}H_{33}N_6O_3S]^+$: 557.2329; found: 557.2335 $[M + H]^+$.

Synthesis of 1,3,3-trimethyl-2-(3-(1,3,3-trimethyl-5-((*E*)-2-(6-methyl-1,2,4,5-tetrazin-3-yl)vinyl)indolin-2-ylidene)prop-1-en-1-yl)-3*H*-indol-1-ium formate (3b). A mixture of cyanine **6b** (30 mg, 0.0492 mmol, 1.0 equiv.), 2-(6-methyl-1,2,4,5-tetrazin-3-yl)ethyl methanesulfonate[19] (32 mg, 0.1475 mmol, 3.0 equiv.), $Pd_2(dba)_3$ (2.3 mg, 0.0025 mmol, 0.05 equiv.), QPhos (2.0 mg, 0.0025 mmol, 0.05 equiv.), *N*,*N*-dicyclohexylmethylamine (32 μL, 0.1475 mmol, 3.0 equiv.) and 1 mL of anhydrous dimethylformamide was purged with N_2 for 15 minutes. The reaction mixture was stirred at 100 °C for 30 minutes. The solvent was evaporated *in vacuo* and the crude product was purified by flash chromatography on silica gel (dichloromethane–methanol 0 to 15%). Before spectroscopic measurements, the product was further purified by preparative HPLC (water–acetonitrile starting from 95 : 5 to 0 : 100) to yield 13.4 mg (52%) of purple crystals. ^{1}H NMR (500 MHz, CD_3OD) δ 8.54 (t, J = 13.5 Hz, 1H), 8.31 (d, J = 16.2 Hz, 1H), 8.00 (s, 1H), 7.79 (d, J = 7.9 Hz, 1H), 7.60–7.52 (m containing: 7.57 (d, J = 16.1 Hz, 1H), 7.54 (d, J = 7.0 Hz, 1H)), 7.44 (d, J = 7.5 Hz, 1H), 7.38 (d, J = 3.6 Hz, 1H), 7.36 (d, J = 4.1 Hz, 1H), 7.32 (t, J = 7.4 Hz, 1H), 6.47 (d, J = 13.6 Hz, 1H), 6.39 (d, J = 13.3 Hz, 1H), 3.69 (s, 3H), 3.65 (s, 3H), 2.96 (s, 3H), 1.80 (s, 6H), 1.75 (s, 6H). ^{13}C NMR (126 MHz, CD_3OD) δ 177.5, 176.0, 167.7, 166.1, 159.7, 152.2, 145.7, 144.0, 142.9, 142.3, 140.9, 134.2, 131.1, 130.0, 127.2, 123.5, 122.5, 121.5, 112.7, 112.4, 104.9, 103.9, 50.9, 50.2, 32.0, 28.3, 28.0, 21.1. HRMS: *m*/*z* calcd for $[C_{30}H_{33}N_6]^+$: 477.2767; found: 477.2762 $[M + H]^+$.

Spectroscopic characterization

Photophysical measurements were performed on a JASCO FP 8300 spectrofluorometer and a JASCO v750 spectrophotometer. A stock solution was prepared in DMSO from the solid dyes

(1 mM). All experiments were conducted in all-sodium PBS (pH = 7.4, containing 0.1% SDS), in order to prevent aggregation. All of the dyes (1 mM in DMSO) were reacted with (1*R*,8*S*,9*S*)-bicyclo[6.1.0]non-4-yn-9-ylmethanol (BCN) in DMSO at room temperature. The completion of the reaction was verified by HPLC-MS. Excitation and emission spectra were recorded using 1 μM concentration of the compounds while absorbance spectra were recorded using 5 μM concentration (DMSO content was kept below 1% in each case). The excitation and emission wavelengths are given for each spectrum. Quantum yields were determined using rhodamine B as a standard. For excitation, emission and absorbance spectra, see Fig. S1–S6 in the ESI.†

Protein labeling

Cell culture. HEK293T (ATCC CRL-3216) and COS-7 (Sigma 87021302) cells were maintained in Dulbecco's modified Eagle's medium (DMEM, Gibco 41965-039) supplemented with 10% FBS (Gibco 10500-064), 1% penicillin–streptomycin (Gibco 15140-122), 1% sodium pyruvate (Life Technologies, Gibco 11360-070) and 1% Glutamax (Gibco 35050-061). The cells were cultured at 37 °C in a 5% CO_2 atmosphere and passaged – using trypsin (0.05%; Gibco 25300-054) – every 3–4 days up to 20 passages.

Bioorthogonal labeling of live cells. HEK293T (40 000 cell per well) or COS-7 (15 000 cell per well) cells were transferred into μ-Slide 8-well plates (Ibidi 80827) and were incubated for 40 h at 37 °C in a 5% CO_2 atmosphere. In the case of HEK293T cells, Ibidi plates were pre-treated with 0.01 mg mL^{-1} poly-L-lysine (Sigma P5899) for 4 hours at room temperature and washed afterwards. The bioorthogonally reactive chemical reporter BCN was administered in the HaloTag substrate or in non-canonical amino acid (ncAA). Therefore, cells were transfected with 0.25 μg of Lamin-HaloTag[32] plasmid using the JetPrime (Polyplus 114-07) transfection agent for four hours according to the manufacturer's protocol. A similar procedure was carried out for ncAA installation. Cells were incubated with 0.25 μg of $IR^{K676TAG}$–GFP [obtained from EMBL under a Material Transfer Agreement][33] or 0.25 μg of $vimentin^{N116TAG}$–GFP[34] in combination with 0.25 μg of the $tRNA^{Pyl}$/NES–$PylRS^{AF}$ plasmid (obtained from EMBL under a Material Transfer Agreement)[35] in the presence of 250 μM BCN^{endo}–lysine (Sichem SC-8014) during transfection. Subsequently, the supernatant was replaced with ncAA-free medium overnight. One day after transfection, cells were labeled with the fluorescent dyes **1a**, **1b**, **3a** and **3b** at a concentration of 1–3 μM in complete DMEM (Gibco 21063-029) for 90 min at 37 °C in the dark. In the case of the HaloTag fusion protein, the Halo–BCN substrate (3 μM; 60 min)[32] was added to the cells before the fluorescent labeling step. Afterwards, a two-hour washing step – with complete DMEM – was performed followed by fixation (4% PFA for 10 min at 25 °C) and quick washes – twice – with PBS prior to imaging.

Confocal and STED imaging and analysis

Confocal and STED images were acquired on a Leica TCS SP8 STED 3× microscope using the 488 nm laser for excitation of the reporter fluorescent protein, 552 nm laser for the probes and 660 nm STED (1.5 W, continuous wave) laser for depletion (at 1.17–2.48 × 10^9 W mm^{-2} nominal intensity with an output laser power of 1.2 W/32 nm × 32 nm pixel size). The images were captured using a Leica HC PL APO 100×/1.40 oil immersion objective using the Leica HyD detector. Spectral detection parameters were set as follows: excitation: 488 nm/em. range: 500–550 nm for GFP and excitation: 552 nm/em. range: 565–650 nm for compounds **1a**, **1b**, **3a**, and **3b**.

Using the Huygens Professional software (SVI), we performed deconvolution for image restoration on the recorded STED images. The deconvolution process was based on the theoretical point spread function (PSF). Images were analysed using Leica Application Suite X and Fiji for ImageJ software (NIH). We selected the results of some representative line analysis for demonstration. A non-linear Gaussian curve was fitted to the normalized fluorescence intensity values using OriginPro 9 software. For characterizing the resolution efficiency, the full width at half maximum values (FWHM) were provided.

Author contributions

EA conducted the synthesis and purification of all starting components and conducted all the characterization studies. EA, GK and PK came up with the experimental design. KN designed the cellular experiments. EA and KN carried out the cellular and labeling studies. GK performed the theoretical calculations. EA, KN, GK and PK wrote the manuscript and created the figures. All authors discussed and provided comments on the manuscript.

Conflicts of interest

There are no conflicts to declare.

Acknowledgements

The present work was supported by the National Research, Development and Innovation Office of Hungary (NKFIH-K-143581 and VEKOP-2.3.3-15-2016-00011). We are also grateful for the generous support from the Eötvös Loránd Research Network (FIKU). We thank Dr György Török for his valuable help in image processing.

References

1 P. Shieh, V. T. Dien, B. J. Beahm, J. M. Castellano, T. Wyss-Coray and C. R. Bertozzi, *J. Am. Chem. Soc.*, 2015, **137**, 7145–7151.
2 S. K. Choi, J. Kim and E. Kim, *Molecules*, 2021, **26**, 1868.
3 E. Kozma and P. Kele, *Org. Biomol. Chem.*, 2019, **17**, 215–233.

4 T. Plass, S. Milles, C. Koehler, J. Szymański, R. Mueller, M. Wießler, C. Schultz and E. A. Lemke, *Angew. Chem., Int. Ed.*, 2012, **51**, 4166–4170.
5 G. V. Los, L. P. Encell, M. G. Mcdougall, D. D. Hartzell, N. Karassina, D. Simpson, J. Mendez, K. Zimmerman, P. Otto, G. Vidugiris and J. Zhu, *ACS Chem. Biol.*, 2008, **3**, 373–382.
6 A. Gautier, A. Juillerat, C. Heinis, I. R. Corrêa, M. Kindermann, F. Beaufils and K. Johnsson, *Chem. Biol.*, 2008, **15**, 128–136.
7 A. Keppler, S. Gendreizig, T. Gronemeyer, H. Pick, H. Vogel and K. Johnsson, *Nat. Biotechnol.*, 2003, **21**, 86–89.
8 K. Lang and J. W. Chin, *Chem. Rev.*, 2014, **114**, 4764–4806.
9 A. I. König, R. Sorkin, A. Alon, D. Nachmias, K. Dhara, G. Brand, O. Yifrach, E. Arbely, Y. Roichman and N. Elia, *Nanoscale*, 2020, **12**, 3236–3248.
10 A. C. Knall and C. Slugovc, *Chem. Soc. Rev.*, 2013, **42**, 5131–5142.
11 B. L. Oliveira, Z. Guo and G. J. L. Bernardes, *Chem. Soc. Rev.*, 2017, **46**, 4895–4950.
12 L. G. Meimetis, J. C. T. Carlson, R. J. Giedt, R. H. Kohler and R. Weissleder, *Angew. Chem., Int. Ed.*, 2014, **53**, 7531–7534.
13 J. C. T. Carlson, L. G. Meimetis, S. A. Hilderbrand and R. Weissleder, *Angew. Chem., Int. Ed.*, 2013, **52**, 6917–6920, DOI: **10.1002/anie.201301100**.
14 A. Wieczorek, P. Werther, J. Euchner and R. Wombacher, *Chem. Sci.*, 2017, **8**, 1506–1510.
15 S. T. Shen, W. Zhang, P. Yadav, X. W. Sun and X. Liu, *Mater. Chem. Front.*, 2023, **7**, 1082–1092.
16 N. K. Devaraj, S. Hilderbrand, R. Upadhyay, R. Mazitschek and R. Weissleder, *Angew. Chem., Int. Ed.*, 2010, **49**, 2869–2872.
17 J. Yang, J. Šečkute, C. M. Cole and N. K. Devaraj, *Angew. Chem., Int. Ed.*, 2012, **51**, 7476–7479.
18 G. Knorr, E. Kozma, A. Herner, E. A. Lemke and P. Kele, *Chem. – Eur. J.*, 2016, **22**, 8972–8979.
19 H. Wu, J. Yang, J. Šečkutė and N. K. Devaraj, *Angew. Chem.*, 2014, **126**, 5915–5919.
20 Y. Lee, W. Cho, J. Sung, E. Kim and S. B. Park, *J. Am. Chem. Soc.*, 2018, **140**, 974–983.
21 G. Knorr, E. Kozma, J. M. Schaart, K. Németh, G. Török and P. Kele, *Bioconjugate Chem.*, 2018, **29**, 1312–1318.
22 E. Németh, G. Knorr, K. Németh and P. Kele, *Biomolecules*, 2020, **10**, 397, DOI: **10.3390/biom10030397**.
23 E. Kozma, G. Estrada Girona, G. Paci, E. A. Lemke and P. Kele, *Chem. Commun.*, 2017, **53**, 6696–6699.
24 P. Werther, K. Yserentant, F. Braun, K. Grußmayer, V. Navikas, M. Yu, Z. Zhang, M. J. Ziegler, C. Mayer, A. J. Gralak, M. Busch, W. Chi, F. Rominger, A. Radenovic, X. Liu, E. A. Lemke, T. Buckup, D. P. Herten and R. Wombacher, *ACS Cent. Sci.*, 2021, **7**, 1561–1571.
25 E. Albitz, D. Kern, A. Kormos, M. Bojtár, G. Török, A. Biró, Á. Szatmári, K. Németh and P. Kele, *Angew. Chem., Int. Ed.*, 2022, **61**, e202111855.
26 L. Chen, F. Li, Y. Li, J. Yang, Y. Li and B. He, *Chem. Commun.*, 2022, **58**, 298–301.
27 W. Mao, W. Chi, X. He, C. Wang, X. Wang, H. Yang, X. Liu and H. Wu, *Angew. Chem., Int. Ed.*, 2022, **61**, e202117386.
28 M. Bojtár, K. Németh, F. Domahidy, G. Knorr, A. Verkman, M. Kállay and P. Kele, *J. Am. Chem. Soc.*, 2020, **142**, 15164–15171.
29 L. Chen, F. Li, M. Nandi, L. Huang, Z. Chen, J. Wei, W. Chi, X. Liu and J. Yang, *Dyes Pigm.*, 2020, **177**, 108313.
30 K. Klehs, C. Spahn, U. Endesfelder, S. F. Lee, A. Fürstenberg and M. Heilemann, *ChemPhysChem*, 2014, **15**, 637–641.
31 M. I. Sorour, K. A. Kistler, A. H. Marcus and S. Matsika, *J. Phys. Chem. A*, 2021, **125**, 7852–7866.
32 Á. Szatmári, G. B. Cserép, T. Á. Molnár, B. Söveges, A. Biró, G. Várady, E. Szabó, K. Németh and P. Kele, *Molecules*, 2021, **26**, 4988.
33 I. Nikic, J. H. Kang, G. E. Girona, I. V. Aramburu and E. A. Lemke, *Nat. Protoc.*, 2015, **10**, 780–791.
34 A. Egyed, A. Kormos, B. Söveges, K. Németh and P. Kele, *Bioorg. Med. Chem.*, 2020, **28**, 115218.
35 I. Nikić, G. E. Girona, J. H. Kang, G. Paci, S. Mikhaleva, C. Koehler, N. V. Shymanska, C. Ventura Santos, D. Spitz and E. A. Lemke, *Angew. Chem., Int. Ed.*, 2016, **55**, 16172–16176.